Metallography, Microstructure, and Analysis (2021) 10:148–157
https://doi.org/10.1007/s13632-021-00730-0

TECHNICAL ARTICLE

Microstructure Evolution and Thermal Stability of AZ31 Alloy Deformed by Multi-Pass DSR

Lucyana D. Larasati[1]

Received: 21 December 2020 / Revised: 26 February 2021 / Accepted: 3 March 2021 / Published online: 31 March 2021

Abstract

Experiments were conducted to investigate the microstructural evolution of AZ31 alloy when deformed by multi-pass differential speed rolling (DSR) using the simplest modification of route A passing sequence. Microstructural observations were taken on all three planes of the sample to obtain a three-dimensional view. Based on quantitative microstructural analysis, the counts of the fine DRX grains increased with increasing number of DSR passes, while the fine DRX grains' size was consistent in each pass. These results signified that the refinery process was attributed to dynamic recrystallization. Thermal stability was perceived by examining the evolution in microstructure and microhardness value of the 4-pass DSR sample during isochronal annealing over a range of temperature from 423 to 723 K. The increase in distortion energy with multi-pass DSR resulted in the decrease in critical temperature for the initiation of recrystallization upon annealing at 423 K, which induced an immediate drop in microhardness.

Keywords Severe plastic deformation · Route A · AZ31 alloy · Microstructural evolution · Thermal stability

Introduction

Severe plastic deformation (SPD) techniques have been flourishing for the past three decades in producing ultra-fine grain size and in enhancing the strength of bulk polycrystalline metals. Well-established methods of SPD for imposing intense plastic strains include equal-channel angular pressing (ECAP), high-pressure torsion (HPT), and accumulative roll bonding (ARB). Despite producing interesting properties, the small dimension of the specimen becomes a principal disadvantage for the broader use of these traditional SPD techniques. Because of this limitation, the processed materials are mostly utilized in modern micro-size specialized industrial branches [1].

Currently, several procedures of SPD techniques are available beside the aforementioned primary techniques. Differential speed rolling (DSR) procedure is one of the powerful non-traditional SPD techniques effective in obtaining an excellent grain refinement practical for manufacturing large bulk sheets. DSR utilizing different rotational speeds amidst its two working rolls is an extent of asymmetric rolling (ASR) that earns more deformation stability than the other asymmetrical procedures like DSR with differently sized rolls or single roller drive rolling (SRDR) [2, 3]. Friction between the sheet and the upper and lower rolls rotating at different angular velocities substantially strengthens the shear deformation effect that promotes extreme grain refinement. Due to this, as the SPD method by ECAP deforms by shearing [4], shear deformation is also the primary deformation mode in DSR [5, 6] aside from the deformation in plane-strain compression, since a reasonable shear component is introduced throughout the thickness [6]. In DSR, the volume that is affected by shear is firmly material-dependent [7]. Among the considerable investigations attempted to utilize DSR, extensive efforts have been devoted to the microstructural design of light metal structural materials of magnesium alloys. Justification for this interest lies in the fact that grain refinement contributes significantly to the strength of hexagonal close-packed (h.c.p.) structure, as per the Hall–Petch equation. Because of this, changing deformation routes is a candidate for grain refinement [8] and is therefore an essential experimental factor in diversifying the microstructure and mechanical properties [9]. This is because small variations in the parameters of the deformation route may lead to a wide variation of grain boundary

✉ Lucyana D. Larasati
lucyana.d.l@ugm.ac.id

[1] Department of Nuclear Engineering and Engineering Physics, Universitas Gadjah Mada, Yogyakarta, Indonesia

distributions and grain size, thus conferring the microstructure significantly different properties.

Numerous works were performed in search of an optimal deformation route using the SPD technique. Recently, Lee discovered in single-roll angular-rolling (SRAR) that grain refinement was preferentially activated in route A rather than in route C [10]. The absence of redundant strain and the accumulated shear deformation by increased number of passes in route A was found to be more effective in intensifying strain partitioning and microstructural heterogeneities than route C, leading to a superior tensile strength after 6-pass processing. In fact, route A has been demonstrated to be the most effective path in equal-channel angular extrusion (ECAE) to form a submicrometer grain structure [11]. Remarkable improvement in refinement and homogeneity of microstructure was also accomplished by varying processing routes using DSR [12]. In the previous work, an ultrafine AZ31 alloy grain size of ~2 μm was achieved after 70% reduction in one rolling pass of DSR [13]. A single-pass rolling deformation to a large thickness reduction requires a high-capacity rolling machine [14]. To reduce the consumption energy level needed for a large rolling force and for torque to reach a high thickness reduction, therefore, multi-pass DSR deformation was applied in this study. Route A passing sequence was chosen since it provides the simplest modification of continuous forming and large-scale processing compared with other techniques and it can be used efficiently in many feasible applications [15].

The parameter settings for the present DSR were made similar to that of DSR in one rolling pass to compare the results of the two. However, unlike in that previous work, the sample was fully lubricated before DSR in the current experiment to minimize friction and adhesion to the roll surface [16]. Development of the corresponding microstructures on the three orthogonal planes was examined, and the influence of thermal exposure on the grain size and microhardness of the final DSR-deformed sample were discussed.

Experimental Procedures

The material used in this study was AZ31 alloy sheet of 4 mm in thickness. The chemical composition in weight% of this alloy is listed in Table 1.

Before DSR deformation, the as-received material was machined into sheets with dimensions of (90 × 40 × 4) mm. The sheets were then homogenized and treated at 673 K (400 °C) for 24 h, followed by air cooling to obtain the initial (0-pass) material. The microstructure of the initial AZ31 alloy shown in Fig. 3a consists of a large fraction of coarse grains and a small fraction of smaller grains with a mean grain size of ~35 μm, as measured in a larger domain image from the preliminary study [17].

DSR deformation was conducted using the identical rolls configuration, and the roll radii were measured to be 110 mm. The roll speed ratio was set to 1:3 ($R_v = 3$) for the lower and upper rolls, respectively, and the lower roll maintained a velocity of 5 rpm. A schematic drawing of DSR method for performing the SPD experiment with the defined x, y, and z orthogonal coordinates of the working space is illustrated in Fig. 1.

AZ31 alloy samples were preheated at 473 K (200 °C) for 15 min prior to DSR deformation. Warm rollers were kept under the same pre-heating temperature during the deformation process because the grain size was found smaller after every additional DSR pass at the deformation temperature of 473 K (200 °C) [12]. Multi-pass DSR was performed in a moderate thickness reduction of 30% per pass, for up to

Table 1 Chemical composition of the AZ31 alloy

Material	Element	Al	Zn	Mn	Si	Fe	Mg
AZ31	wt%	2.89	0.96	0.31	0.12	0.15	Bal.

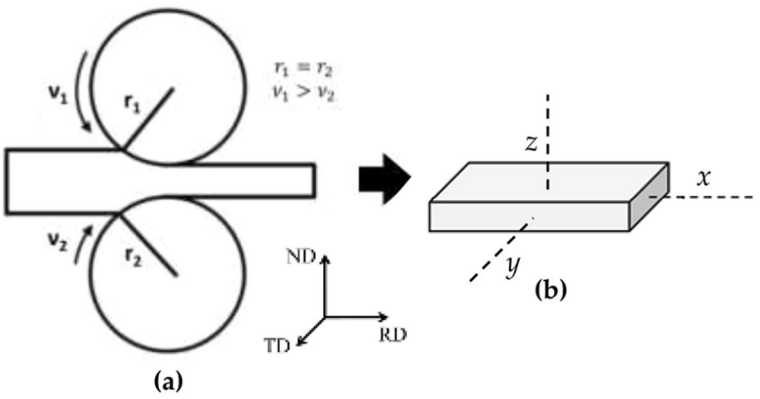

Fig. 1. **a** Schematic drawing of the DSR method and **b** geometry of the working piece

4-pass to a total reduction of 76%. In this way, a comparable deformation degree to that of the high reduction rolling can be obtained through extending the DSR effect by increasing the process pass. To be fair, the sample orientation was maintained between the repetitive processing after 1-pass, 2-pass, and 3-pass, as illustrated in Fig. 2, following the route A passing sequence as referred in the literature.

To evaluate thermal stability, i.e., the ability to retain plastic characteristics under the influence of high temperature and high deformations [18] of the DSR-deformed AZ31 alloy, the 4-pass DSR sample was investigated. Pieces were cut from the 4-pass DSR sample for 1 h annealing treatment at temperatures ranging from 423 K (150 °C) to 723 K (450 °C) with 50 K increments. Microstructures of initial, deformed, and annealed AZ31 alloy samples were analyzed using optical microscopy (OM). An image analysis program of MIPAR was utilized based on optical images to determine grain size distribution and the average grain size were calculated via linear intercept method. Microstructure examination was conducted on all three planes (*x*-, *y*-, and *z*-plane) for the deformed samples (1-pass to 4-pass DSR) and on the *y*-plane for the annealed samples (4-pass DSR). Samples were prepared based on the standard metallography procedure. Etching was carried out with 10 ml acetic acid, 5 g picric acid, 10 ml H_20, and 100 ml ethanol.

To elucidate the effect of thermal exposure after the annealing treatments on the microhardness, Vickers microhardness tests were performed in fifteen separate measurements on the *y*-plane of each annealed sample under a load of 50 g and under 10 s dwell time.

Results and Discussion

Deformation Microstructures

Optical images taken from the three orthogonal planes of the (a) 1-pass, (b) 2-pass, (c) 3-pass, and (d) 4-pass DSR-deformed AZ31 alloy samples are shown in Fig. 3.

Figure 3b shows that microstructural improvement can be attained by DSR. The general overview of the microstructures among the three investigated planes (*x*, *y*, and *z*) exhibited a similar degree of refinement, suggesting that large equivalent strain resulting from compressive strain and additional shear deformation in DSR was fairly distributed along the planes.

After severe deformation of 1-pass DSR at 473 K, the initial AZ31 alloy was changed to a typical heavily cold-rolled structure. No apparent occurrence of dynamic recrystallization (DRX) can be confirmed because determining DRX grains via optical microscopic observation is difficult. Such characteristic was quite different compared to that of AZ31 alloy deformed by symmetric rolling, in which recrystallized grains appeared more visibly after 1-pass deformation [17]. According to the obtained microstructure shown in Fig. 3b, twinning dominant flow intersected with each other and crossed the original grains leading to the segmentation of the initial microstructure into large crossed bands and profuse strips with a large density of needle-like shear bands. This observation without distinct shear banding direction was also reported in other studies [19, 20]. Results from previous studies using lower rotation speed ratios between DSR rolls ($R_v = 1.167$ and $R_v = 1.5$) discovered that the microstructures of Mg alloys exhibited unidirectional shear bands at some inclination angle (20°–30°) with respect to the rolling direction. Meanwhile, the comparison symmetric rolling, i.e., two rolls with similar rotation speed under the same process conditions, exhibited crossed shear bands [19, 20].

Despite implementing a similar DSR configuration and parameters, microstructural characteristic obtained through 1-pass DSR in the present study differs to the obtained micrograph by Jeong et al. [13]. However, optical micrograph reported by Kim et al. [21] revealed flow localization without the occurrence of DRX. Kim et al. implemented different upper and lower DSR rolls diameter configurations and maintained the same rotational speed between the two rolls. Optimum roll diameter ratio was of 1.5 was used to induce shear deformation [21]. Furthermore, high thickness reduction associated with a large amount of deformation was applied. Kim et al. suggested that the formation of such microstructural feature can be related to the rate and amount of deformation during rolling. Meanwhile, new grain structures started to develop in relatively low strain during hot and warm deformation of Mg alloys [22]. Result from Kaseem et al. also supported this theory [23]. Globular grains were shown in the DSR-deformed AZ31 alloy sample after single pass at 473 K when the speed of the lower roll was set to a

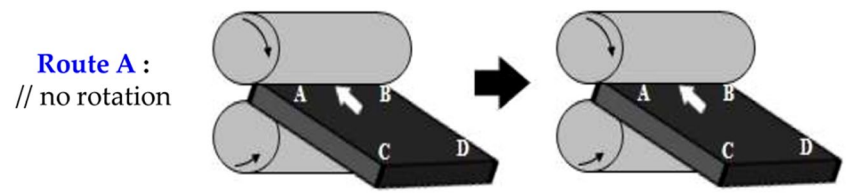

Fig. 2. Schematic illustration of the passing sequence of the DSR deformation

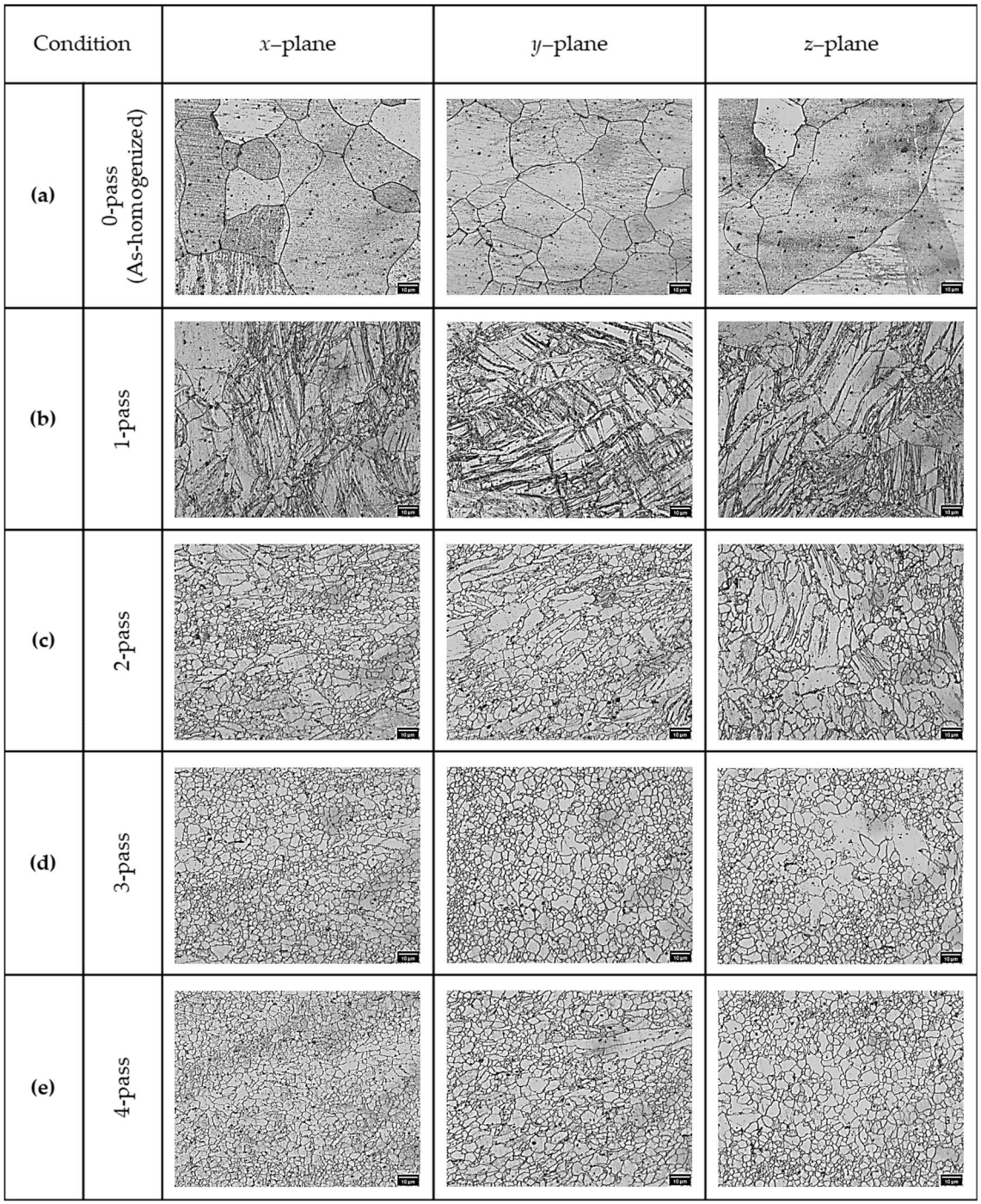

Fig. 3. Microstructures of the AZ31 alloy for: **a** the initial material/0-pass and after DSR deformation through **b** 1-pass, **c** 2-pass, **d** 3-pass, and **e** 4-pass

slower rate (3 rpm) than that utilized in the present study (5 rpm). Therefore, agreeable to the dynamic recrystallization characters during rolling process, the absence of nucleation of new grains and the dominant flow localization in the present microstructure developed because the material underwent a large deformation with a high strain rate [14, 19].

The velocity difference at different positions of DSR-deformed sample was the main factor affecting the distribution of shear band [24]. In order to accommodate the plastic strain arising from shear deformation, twinning as a key

deformation mode for hexagonal closed packed (h.c.p.) Mg systems was generated [20]. The generation of such twinning feature was necessary due to an insufficient number of active slip systems in magnesium. Apart from that, earlier investigations suggested that most of the strain of large grains were accommodated by twinning [25], and that same processing parameters may lead to different structures depending on the nature of the initial material [26]. Thus, a relatively large initial AZ31 alloy grain should be taken into account to the enhanced twinning activity, considering a higher propensity for twinning is expected more with coarse grain size than with the finer initial grains [27]. The distribution formation of the grains within the *x*-, *y*-, and *z*-plane microstructures during 1-pass DSR is provided in Fig. 4.

The 1-pass DSR sample exhibits a broad distribution of grain sizes ranging from 0.75 to ~22 μm, with an average grain size of 2.66 μm.

As described in earlier research [28], when the cumulative strain increased in the deformation process where the boundaries were extended in one direction, such as in the current DSR that implementing route A passing sequence, the original high angle boundaries and the new deformation-induced boundaries rotated and developed a fibrous structure primarily containing aligned lamellar grains oriented with the longer axes of the grain. The resulting convergence of the transverse spacing of these lamellar involved some break-up of the grains producing shorter lengths and lower aspect ratio grains that slowly spheroidized. Nonetheless, if the accumulated strain was not enough, the incomplete fragmentation of coarse grain occurred, leading to some a few remaining poorly refined areas. Consequently, significant variation in grain size followed. Observation to this explanation can be well seen in the microstructure after the 2-pass DSR in Fig. 3. The acquired microstructure in Fig. 3c shows a mixture of rounded twin-free grains with sizes of 1–2 μm lying within arrays of elongated grains of 6.5 μm in the average size. The figure also shows the dramatic reduction of the volume fraction of deformation twins compared to that in the 1-pass DSR, with only a small proportion observed within the grain boundaries of the remnant coarse grains. The decreasing number of twins can be responsible for a good ductility even after a large improvement in the tensile properties as reported from the study of multi-pass warm-rolled AZ31 alloy [29]. Another particular interest was that within the small grain population, very fine grains of 0.25 μm were detected by means of MIPAR grain analysis software. Accordingly, the grain size distribution changed after the 2-pass due to the emergence of these very fine grains in the microstructure. The corresponding grain size distribution as confirmed by the quantitative analysis on microstructural examination is plotted in Fig. 5.

2-pass DSR still exhibited a broad grain size distribution. However, counts number of small grains of 0.25 μm increased, while counts number of coarser grains reduced. Measured average gave an average grain size in this condition was 2.38 μm. The increasing number of only a few microns of grains resulted in the evolution of the grain size distribution from a bi-modal to a tri-modal type. This improvement of grain refinement could be attributed to the dynamic recrystallization (DRX), which occurred in the area of defect-free grains when the free energy for nucleation was high enough due to the additional pass after the 2-pass DSR. This was consistent to the known fact that the activity of dynamic recrystallization (DRX) and grain-boundary mobility increases with increasing rate of dislocation storage in various metals subjected to severe plastic deformation [30]. It was supposed that the refinery process occurred in the area with twins, and that the development of stress concentrations at the former twins facilitated the grain subdivision by triggering new grain formation along the twin boundaries [31]. Twins disappeared as the new grains emerged. The occurrence of the dynamic recrystallization (DRX) showed

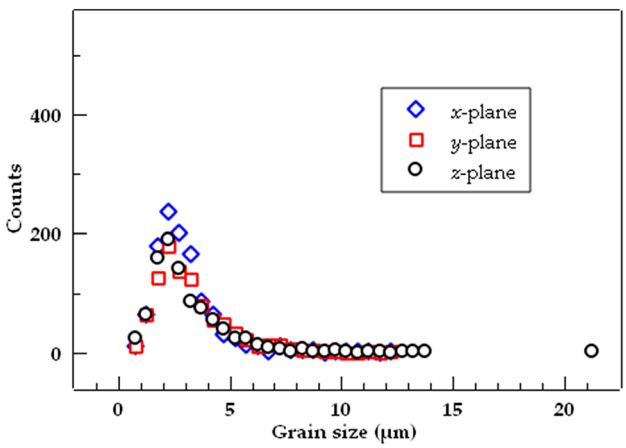

Fig. 4. Distribution of grain size for AZ31 alloy after 1-pass DSR

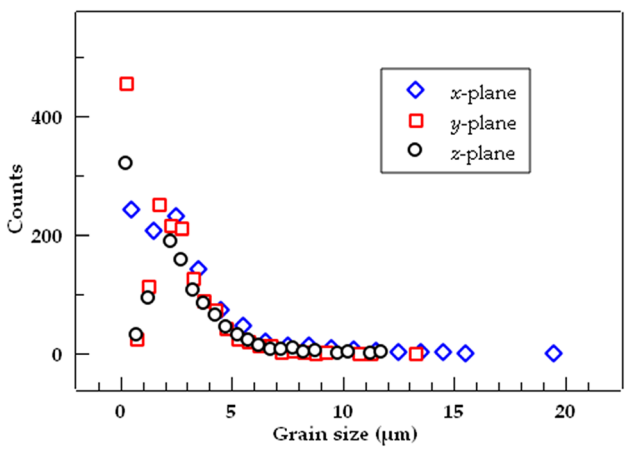

Fig. 5. Distribution of grain size for AZ31 alloy after 2-pass DSR

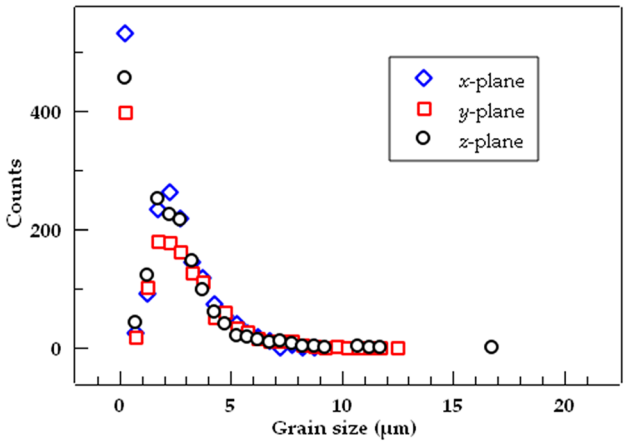

Fig. 6. Distribution of grain size for AZ31 alloy after 3-pass DSR

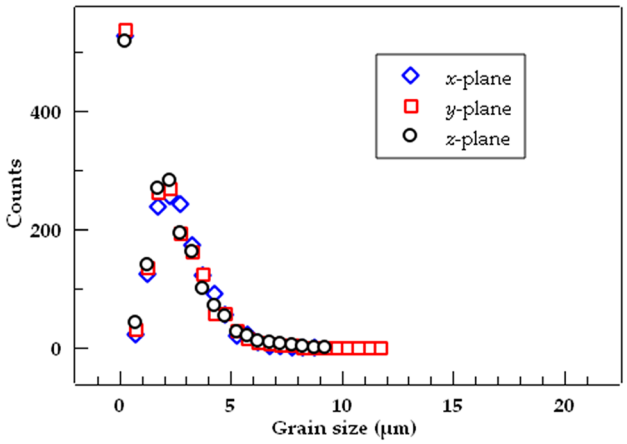

Fig. 7. Distribution of grain size for AZ31 alloy after 4-pass DSR

good correspondence to the grain refinement model of a previously developed magnesium alloy [26].

From Fig. 3d, the microstructure of the 3-pass DSR was more refined compared to the 2-pass DSR. Simultaneous refinement process by successive breaking-up of large grains and progression of DRX prompted a decrease in the overall measured grain size (2.17 μm) albeit the existence of the coarse grains. The grain size distribution after 3-pass DSR is given in Fig. 6.

Numerous new and fine recrystallized grains surrounded the large grains as band. On the other hand, the old large grains were continuously refined to a reasonably more equiaxed shape at the cost of the decrease in elongated grains. Increased number of fine grains (0.25 μm) subsequent DSR pass indicated the effect of an additional shear strain in enhancing the formation of more dynamic recrystallized grains. It is noted that the grain development under DRX making up a necklace structure emerged in narrow regions of shear bands, as can be seen from the microstructure of the *x*-plane. However, the presence of shear band was hardly observed in the *y*- and *z*-plane microstructure. The necklace-like grains probably occupied areas along the traces of the pre-existing boundaries affected by the shear component. Therefore, the inner cores of the coarse grains in the *y*- and *z*-plane were not thoroughly refined. Outstanding grain refinement in certain regions indicated that more intense plastic flow concentrated on certain areas during DSR deformation. Fine DRX grain size was also found to be in the same size to that of preceding DSR pass. The reason behind this might be related to the consequent monotonic shearing from DSR with non-alternating strain path. On each separate DSR pass, cumulative additional strains from the exact same thickness reduction per pass were expected to yield the same size of DRX grains.

DRX process still occurred during the 4-pass DSR. At the same time, recrystallized grains from the previous 3-pass DSR slightly grew. It is apparent from the microstructure in Fig. 3e that the repetitive deformation increased the total grain boundary area. Comparison of the microstructures in *x*-, *y*-, and *z*-plane, however, revealed that a similar grain shape from the preceding structure was maintained in the *z*-plane, while the grain shapes in the *x*- and *y*-plane appeared skewed and became more pancake-shaped, indicating an aspect ratio of more than one order of magnitude. In addition to the prominent role of the processing route, the alteration in this grain shape was also connected to the temperature rise phenomenon during DSR deformation. With more DSR passes, increased strain accumulation should lead to a larger distortion of the crystal lattice and an increase the driving force for recrystallization. Concurrently, the temperature rise in the DSR-deformed sample increases as the sample thickness decrease per pass [32], resulting in the grain coarsening. Thus, by imposing more DSR passes, there was a counteracting effect to the grain refinement process and causing the shape of the grains to broaden in that way to fit the equilibrium structural unit. The evolution of the grain size distribution after the 4-pass DSR is depicted in Fig. 7.

Distribution of grain size was observed in a narrower area, which indicated a more homogeneous grain size. DRX grains with the size of 0.25 μm according to the analysis software were shown to have the highest count occurrence in all the three planes after the 4-pass DSR. This result confirmed that a gradual refinement through several passes up to 4-pass DSR via route A passing sequence attributed partly to the increasing count of smallest grains due to dynamic recrystallization instance during the deformation process. It should be noted that although many grains were refined after the 4-pass DSR, an elongated coarse grain fragment can be observed in the *x*-plane microstructure. A number of studies suggested that this grain survived from the serial deformation by DSR and was found to be resistant to recrystallization [33]. Average grain size (2.06 μm) decreased slightly

from the previous DSR pass, which agrees with literature reports that the grain size does not reduce significantly if the process is conducted at a constant deformation temperature as compared to a process of decreasing deformation temperatures [34].

Evolution of the Deformation Microstructure after Annealing

An earlier report described the influence of static annealing on grain growth in samples of the AZ31 alloy fabricated by constrained groove pressing [35]. In the present investigation, similar observations were obtained on the samples fabricated by DSR deformation. Optical images of a typical 4-pass DSR structure produced without any sample rotation show the corresponding microstructure for each annealing temperature as presented in Fig. 8.

Appreciable recrystallization had occurred just after annealing at 423 K. A significant portion of recrystallized grains was detected and found to coexist with the refined grains that remained from DSR. This was a typical sign that static recrystallization (SRX) took place in a discontinuous mode. Recrystallization temperature of the processed alloy in this study was approximately 423 K. Even lower recrystallization temperature of AZ31 alloy has been reported at 373 K after deformation to 86% total rolling reduction [36]. This behavior can be explained by considering the variations in dislocation density. During deformation process, particularly in severe deformation, a large number of dislocations was generated. In the case of route A passing sequence, where the sample was continuously strained in one principal direction, the location-dependent shear was expected to accumulate monotonically in the same plane and in the same direction. During annealing treatment, rearrangement of grains was attempted to minimize the internal energy stored by recrystallization and grain growth [37]. As a consequence, the severely distorted structure which was formed in some preferred areas resulted in the uneven rate of recrystallization during annealing treatment. In addition, driven by high grain boundary energies of the fine-grained recrystallized structure [35], only a limited grain growth proceeding at a slow pace was observed on the deformed grains.

Annealing to recrystallization, i.e., 423 K, the recrystallizing grains contacted each other, indicating the local completion of recrystallization process. Subsequently, grains started to grow to minimize interfacial energy [38]. Different growth conditions existed for grain growth both in the completely recrystallized area and in the region composed of recrystallized and unrecrystallized grains (recrystallization front). Microstructure was characterized with normal grain growth in the completely recrystallized area. However, at the interface of recrystallized and unrecrystallized grains, a high amount of grain boundary energy was consumed and grain growth spread towards a zone where stored energy is still present [39]. Concurrently, upon annealing at 473 K, grain growth started to take place and the area fraction of smaller grains decreased in favor of larger ones. However, the smaller grains were still distinguishable from the surrounding coarser ones. The relative frequency of small grains was continuously disappearing, and the uniformity of the structure increased substantially as the grains coarsened homogeneously after annealing at 523 K. Figure 8c shows that individual grains are relatively uniform in size.

It has been shown that the significant amount of stored energy also gave rise to decreased annealing temperature for subsequent abnormal grain growth [40]. The incipient

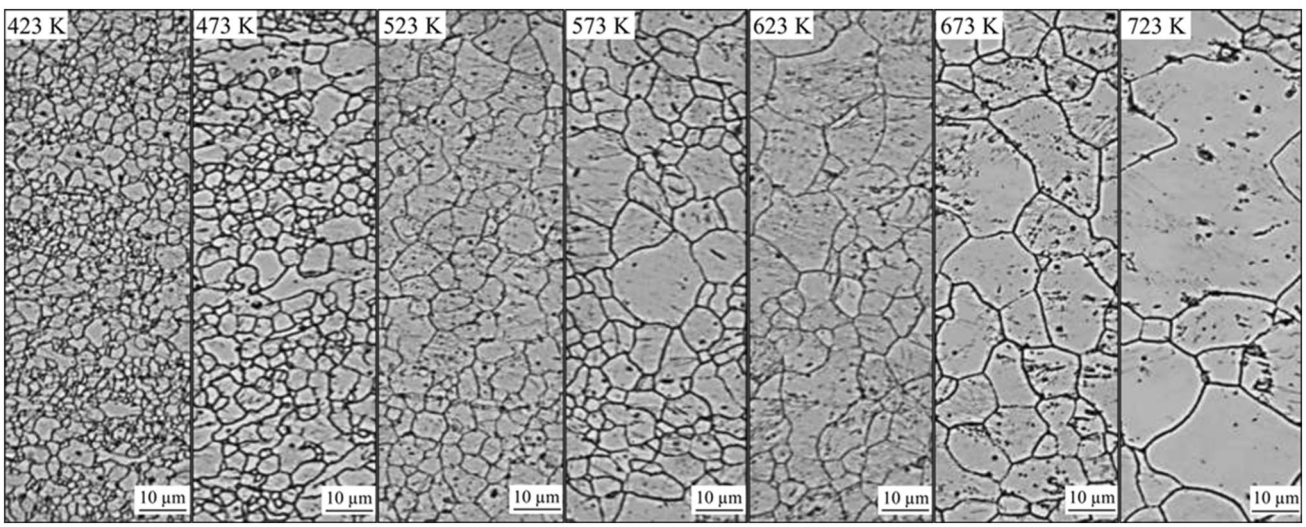

Fig. 8. Optical microstructures of the 4-pass DSR-deformed sample after annealing at: **a** 423 K, **b** 473 K, **c** 523 K, **d** 573 K, **e** 623 K, **f** 673 K, and **g** 723 K

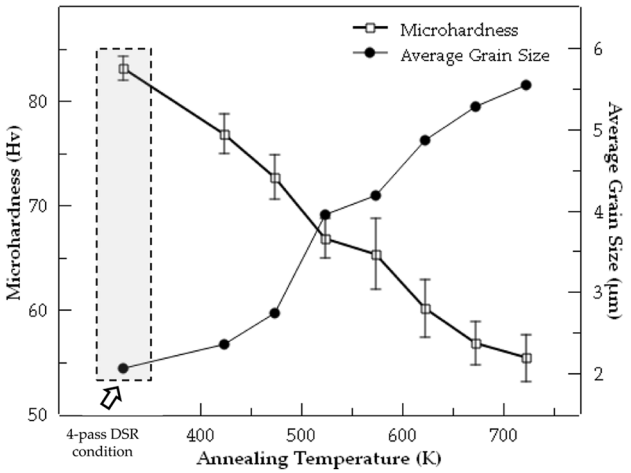

Fig. 9. Microhardness and grain size variations as a function of annealing temperature of the AZ31 alloy after 4-pass DSR deformation.

of secondary or abnormal grain growth was evident in the microstructure after 573 K annealing temperature. The presence of a few grains that grew faster than the others resulted in inhomogeneous grain growth.

At higher annealing temperature of 623 K, the abnormal grain growth was completed and further coarsening of the grains was developed with a normal growing size. Increasing the temperature further to 673 K, rapid grain coarsening became more pronounced since a higher temperature often provides higher boundary mobility [41]. Ultimately, large growing grains were seen throughout the entire sample, and increasing the homogeneity of the structure.

The largely coarse grains seemed to immerge into their neighboring small grains, leading to the formation of much larger grains after a more severe annealing temperature at 723 K. This can be attributed to the significant enhancement of the average atom energy level enabling more atoms to overcome the activation energy barrier for grain growth [42].

Microhardness Evolution During Annealing Experiments

Figure 9 shows the Vickers microhardness (Hv) variation as a function of the annealing temperatures and the corresponding plot of the average grain size measured using the linear intercept method.

Average microhardness value of the 4-pass DSR sample in the first data point was 83.09 Hv. Hv value decreased continuously at elevated temperatures, which conformed to the microstructural observations shown in Fig. 8. The corresponding microhardness values and average grain size of the samples are summarized in Table 2.

Table 2 Microhardness and average grain size of the samples

Processing condition	Microhardness (Hv)	Average grain size (μm)
4-Pass DSR	83.09 ± 1.15	2.06 ± 1.53
After annealing (K)		
423	76.85 ± 1.87	2.35 ± 0.95
473	72.71 ± 2.13	2.74 ± 1.70
523	66.84 ± 1.87	3.95 ± 2.84
573	65.34 ± 3.42	4.18 ± 4.46
623	60.11 ± 2.73	4.86 ± 5.39
673	56.82 ± 2.06	5.27 ± 21.48
723	55.36 ± 2.21	5.54 ± 30.25

The abrupt decrease in microhardness after annealing at 423 K caused by recrystallization phenomena is consistent with the previous report [43]. This result indicated that the produced microstructure by the current DSR method exhibited low thermal stability. Gradual decrease at 473 K annealing temperature coincided with the microstructure observed in the sample. This was ascribed to grain growth, stress relaxation, and an increase in volume fraction of growing grains. Larger drop in microhardness was seen after annealing at 523 K due to the observed marked grain growth in the corresponding microstructure after 523 K. It is obvious because a marked grain growth was observed in the corresponding microstructure after 523 K. Nevertheless, the homogeneity of the microhardness was pretty stable. Some structure coarsening in a heterogeneous manner took place as the annealing temperature went up to 573 K. Increased calculated standard deviation values confirmed the heterogeneous course of the microstructure with the presence of abnormal grain, although the average grain size was almost the same as those of the 523 K. Faster rate of the decrease in the microhardness was observed after 623 K and then slightly slowed down after 673 K. This observation correlated directly with the analysis of the abnormal grain growth. As soon as the annealing temperature reached 723 K, the microhardness approached that of the initial material ≈55.60 Hv.

Conclusions

In this paper, the effects of the route A passing sequence during the deformation via differential speed rolling (DSR) at 473 K on the microstructure evolution and thermal stability of AZ31 Mg alloy were studied. The important observations are:

1. The 1-pass DSR sample has a cold-worked type of microstructure with an extensive amount of deformation twins, which disappear after multi-pass DSR.

2. The average grain sizes through the 1-, 2-, 3-, and 4-pass DSR are 2.66, 2.38, 2.17, and 2.06 μm, respectively.
3. Microstructure of the 4-pass DSR sample with a total of 76% thickness reduction in this study has a similar average grain size to that of DSR with 70% thickness reduction in a single pass (~2 μm), but less homogeneous.
4. Remarkable grain refinement is obtained primarily due to the occurrence of dynamic recrystallization (DRX) during the multi-pass DSR deformation.
5. Comparison of the grain size distribution graphs derived from the optical microstructure analysis revealed that the count of smallest DRX grains increased as the DSR pass number following route A passing sequence (no sample rotation per pass) increased.
6. With greater fraction of DRX grains after each consecutive DSR pass, no significant change in the DRX grain size is observed.
7. The large distortion energy imposed via DSR deformation decreases the critical temperature for the initiation of recrystallization which induces an earlier drop in microhardness upon annealing at 423 K.
8. The subsequent annealing of the resulted 4-pass DSR-deformed sample at temperatures ranging from 423 to 723 K was not thermally stable.

Acknowledgments The author acknowledges the Plasticity Control and Mechanical Modeling Laboratory, School of Materials Science and Engineering, Department of Engineering, Yeungnam University, South Korea, for providing all the means to carry out this work and access to experimental facilities.

Declarations

Conflict of interest The authors declare that they have no conflicts of interest.

References

1. J. Vrátná, M. Janeček, J. Čížek, D.J. Lee, E.Y. Yoon, H.S. Kim, Mechanical properties and microstructure evolution in ultrafine-grained AZ31 alloy processed by severe plastic deformation. J. Mater. Sci. **48**, 4705–4712 (2013). https://doi.org/10.1007/s10853-013-7151-x
2. S.H. Lee, D.N. Lee, Analysis of deformation textures of asymmetrically rolled steel sheets. Int. J. Mech. Sci. **43**, 1997–2015 (2001)
3. Y.G. Ko, Microstructure evolution and mechanical properties of severely deformed Al alloy processed by differential speed rolling. J. Alloys Compd. **536**, S122–S125 (2012). https://doi.org/10.1016/j.jallcom.2011.12.009
4. C.W. Su, L. Lu, M.O. Lai, Mechanical behaviour and texture of annealed AZ31 Mg alloy deformed by ECAP. Mater. Sci. Technol. **23**, 290–296 (2007). https://doi.org/10.1179/174328407X161132
5. Y.G. Ko, J. Suharto, J.S. Lee, B.H. Park, D.H. Shin, Effect of roll speed ratio on deformation characteristics of IF steel subjected to differential speed rolling. Met. Mater. Int. **19**, 603–609 (2013). https://doi.org/10.1007/s12540-013-3033-7
6. J.B. Lee, T.J. Konno, H.G. Jeong, Grain refinement and texture evolution in AZ31 Mg alloys sheet processed by differential speed rolling. Mater. Sci. Eng. B. **161**, 166–169 (2009). https://doi.org/10.1016/j.mseb.2009.02.021
7. J. Romberg, J. Freudenberger, H. Watanabe, J. Scharnweber, A. Eschke, U. Kühn, H. Klauß, C.-G. Oertel, W. Skrotzki, J. Eckert, L. Schultz, Ti/Al multi-layered sheets: differential speed rolling (Part B). Metals. **6**, 31 (2016). https://doi.org/10.3390/met6020031
8. Y.-Q. Zhao, H.-M. Chen, J. Zhang, R. Ma, Y.-D. Liu, Y.-N. Wang, L. Wang, Q. Zhang, W.-G. Li, Influences of asymmetric reduction rolling on the microstructure and mechanical properties of AZ91. Acta Metall. Sin. (Engl. Lett.). **31**, 673–680 (2018). https://doi.org/10.1007/s40195-017-0695-z
9. M. Nagaraj, P. Deena, B. Ravisankar, Thermal stability and mechanical behaviour of equal channel angular pressed structural steel IS2062. Trans. Indian Inst. Met. **72**, 2581–2589 (2019). https://doi.org/10.1007/s12666-019-01727-8
10. H.H. Lee, K.J. Hwang, H.K. Park, H.S. Kim, Effect of processing route on microstructure and mechanical properties in single-roll angular-rolling. Materials. **13**, 2471 (2020). https://doi.org/10.3390/ma13112471
11. A. Gholinia, P.B. Prangnell, M.V. Markushev, The effect of strain path on the development of deformation structures in severely deformed aluminium alloys processed by ECAE. Acta Mater. **48**, 1115–1130 (2000). https://doi.org/10.1016/S1359-6454(99)00388-2
12. Y.H. Ji, J.J. Park, Analysis of thermo-mechanical process occurred in magnesium alloy AZ31 sheet during differential speed rolling. Mater. Sci. Eng. A. **485**, 299–304 (2008)
13. H.G. Jeong, Y.G. Jeong, W.J. Kim, Microstructure and superplasticity of AZ31 sheet fabricated by differential speed rolling. J. Alloys Compd. **483**, 279–282 (2009). https://doi.org/10.1016/j.jallcom.2008.08.130
14. W.J. Kim, S.J. Yoo, H.T. Jeong, D.M. Kim, B.H. Choe, J.B. Lee, Effect of the speed ratio on grain refinement and texture development in pure Ti during differential speed rolling. Scr. Mater. **64**, 49–52 (2011). https://doi.org/10.1016/j.scriptamat.2010.09.002
15. A. Vinogradov, T. Ishida, K. Kitagawa, V. Kopylov, Effect of strain path on structure and mechanical behavior of ultra-fine grain Cu–Cr alloy produced by equal-channel angular pressing. Acta Mater. **53**, 2181–2192 (2005). https://doi.org/10.1016/j.actamat.2005.01.046
16. H. Watanabe, T. Mukai, K. Ishikawa, Differential speed rolling of an AZ31 magnesium alloy and the resulting mechanical properties. J. Mater. Sci. **39**, 1477–1480 (2004). https://doi.org/10.1023/B:JMSC.0000013922.16079.d3
17. M. Kaseem, B.K. Chung, H.W. Yang, K. Hamad, Y.G. Ko, Effect of deformation temperature on microstructure and mechanical properties of AZ31 Mg alloy processed by differential-speed rolling. J. Mater. Sci. Technol. **31**, 498–503 (2015). https://doi.org/10.1016/j.jmst.2014.08.016
18. M.V. Maltsev, T.N. Volkova, Thermal stability of cold-worked titanium alloys. Met. Sci. Heat Treat. Met. (Engl. Transl.); (United States). **27**, 1–2 (1985). https://doi.org/10.1007/BF00741891
19. X. Huang, K. Suzuki, M. Yuasa, Y. Chino, Effects of initial microstructure on the microstructural evolution and stretch formability of warm rolled Mg–3Al–1Zn alloy sheets. Mater. Sci. Eng. A. **587**, 150–160 (2013)

20. C.W. Su, L. Lu, M.O. Lai, A model for the grain refinement mechanism in equal channel angular pressing of Mg alloy from microstructural studies. Mater. Sci. Eng. A. **434**, 227–236 (2006)
21. S.-H. Kim, B.-S. You, C. Dong Yim, Y.-M. Seo, Texture and microstructure changes in asymmetrically hot rolled AZ31 magnesium alloy sheets. Mater. Lett. **59**, 3876–3880 (2005). https://doi.org/10.1016/j.matlet.2005.07.024
22. X. Yang, H. Miura, T. Sakai, Isochronal annealing behavior of magnesium alloy AZ31 after hot deformation. Mater. Trans. **46**, 2981–2987 (2005). https://doi.org/10.2320/matertrans.46.2981
23. M. Kaseem, H.W. Yang, K. Hamad, Y.G. Kim, B.H. Park, Y.G. Ko, Microstructure and plastic anisotropy of fine grained AZ31 magnesium alloy fabricated by differential speed rolling at 473 and 573 K. Mater. Res. Innov. **19**, S5-477-S5-480 (2015). https://doi.org/10.1179/1432891714Z.0000000001135
24. B. Xiao, J. Song, A. Tang, B. Jiang, W. Sun, Q. Liu, H. Zhao, F. Pan, Effect of pass reduction on distribution of shear bands and mechanical properties of AZ31B alloy sheets prepared by on-line heating rolling. J. Mater. Process. Technol. **280**, 116611 (2020). https://doi.org/10.1016/j.jmatprotec.2020.116611
25. R. Ma, Y. Zhao, Y. Wang, Grain refinement and mechanical properties improvement of AZ31 Mg alloy sheet obtained by two - stage rolling. Mater. Sci. Eng. A. **691**, 81–87 (2017). https://doi.org/10.1016/j.msea.2017.02.107
26. R.B. Figueiredo, T.G. Langdon, Grain refinement and mechanical behavior of a magnesium alloy processed by ECAP. J Mater Sci. **45**, 4827–4836 (2010). https://doi.org/10.1007/s10853-010-4589-y
27. B. Schuh, F. Mendez-Martin, B. Völker, E.P. George, H. Clemens, R. Pippan, A. Hohenwarter, Mechanical properties, microstructure and thermal stability of a nanocrystalline CoCrFeMnNi high-entropy alloy after severe plastic deformation. Acta Mater. **96**, 258–268 (2015). https://doi.org/10.1016/j.actamat.2015.06.025
28. P.B. Prangnell, J.R. Bowen, M. Berta, P.J. Apps, P.S. Bate, Stability of ultra-fine 'grain structures' produced by severe deformation. Mater. Sci. Forum. **467–470**, 1261–1270 (2004). https://doi.org/10.4028/www.scientific.net/MSF.467-470.1261
29. S.V.S.N. Murty, N. Nayan, S.C. Sharma, K.S. Kumar, P.P. Sinha, Development of ultrafine-grained magnesium alloy AZ31 by multi-pass warm rolling. Met Sci Heat Treat. **53**, 270–273 (2011). https://doi.org/10.1007/s11041-011-9381-3
30. W. Wang, Q. Miao, X. Chen, Y. Yu, W. Zhang, W. Chen, E. Wang, Critical rolling process parameters for dynamic recrystallization behavior of AZ31 magnesium alloy sheets. Materials. **11**, 2019 (2018). https://doi.org/10.3390/ma11102019
31. D. Sagapuram, M. Efe, W. Moscoso, S. Chandrasekar, K.P. Trumble, Controlling texture in magnesium alloy sheet by shear-based deformation processing. Acta Mater. **61**, 6843–6856 (2013). https://doi.org/10.1016/j.actamat.2013.07.063
32. R.B. Megantoro, Y.G. Ko, Temperature rise during differential speed rolling. J. Alloys Compd. **586**, S254–S257 (2014). https://doi.org/10.1016/j.jallcom.2012.11.173
33. P. Molnár, A. Jäger, P. Lej, Effect of temperature on grain refinement of Mg-3Al-1Zn alloy processed by equal channel angular pressing. Acta Phys. Pol. A. **122**, 461–464 (2012). https://doi.org/10.12693/APhysPolA.122.461
34. K.S. Fong, M.J. Tan, B.W. Chua, D. Atsushi, Enabling wider use of magnesium alloys for lightweight applications by improving the formability by groove pressing. Procedia CIRP. **26**, 449–454 (2015). https://doi.org/10.1016/j.procir.2014.07.031
35. K. Soon Fong, M. Jen Tan, F. Lan Ng, A. Danno, B. Wah Chua, Microstructure stability of a fine-grained AZ31 magnesium alloy processed by constrained groove pressing during isothermal annealing. J Manuf Sci Eng. **139**, 081007 (2017). https://doi.org/10.1115/1.4036529
36. W. Qiu, E. Han, L. Liu, Effect of heat treatment on microstructures and mechanical properties of extruded-rolled AZ31 Mg alloys. Trans. Nonferrous Met. Soc. **20**, s481–s487 (2010). https://doi.org/10.1016/S1003-6326(10)60523-7
37. M. Thein, L. Lu, M. Lai, Kinetics of grain growth in nanocrystalline magnesium-based metal–metal composite synthesized by mechanical alloying. Compos. Sci. Technol. **66**, 531–537 (2006). https://doi.org/10.1016/j.compscitech.2005.07.002
38. P. Cao, L. Lu, M.O. Lai, Grain growth and kinetics for nanocrystalline magnesium alloy produced by mechanical alloying. Mater. Res. Bull. **36**, 981–988 (2001). https://doi.org/10.1016/S0025-5408(01)00578-5
39. X. Song, M. Rettenmayr, C. Müller, H.E. Exner, Modeling of recrystallization after inhomogeneous deformation. Metall. Mat. Trans. A. **32**, 2199–2206 (2001). https://doi.org/10.1007/s11661-001-0195-6
40. H. Sun, H. Chao, E. Wang, Microstructure stability of cold drawn AZ31 magnesium alloy during annealing process. Trans. Nonferrous Met. Soc. **21**, S215–S221 (2011). https://doi.org/10.1016/S1003-6326(11)61581-1
41. W.J. Kim, B.G. Hwang, M.J. Lee, Y.B. Park, Effect of speed-ratio on microstructure, and mechanical properties of Mg–3Al–1Zn alloy, in differential speed rolling. J. Alloys Compd. **509**, 8510–8517 (2011). https://doi.org/10.1016/j.jallcom.2011.05.063
42. Q. Miao, L. Hu, X. Wang, E. Wang, Grain growth kinetics of a fine-grained AZ31 magnesium alloy produced by hot rolling. J. Alloys Compd. **493**, 87–90 (2010). https://doi.org/10.1016/j.jallcom.2009.12.049
43. L.R.C. Malheiros, R.B. Figueiredo, T.G. Langdon, Grain size and microhardness evolution during annealing of a magnesium alloy processed by high-pressure torsion. J. Mater. Res. Technol. **4**, 14–17 (2015). https://doi.org/10.1016/j.jmrt.2014.10.008